https://doi.org/10.1016/j.jobe.2023.107195

Improving the performance of indirect evaporative cooler for energy recovery from the perspective of nozzle configuration: A CFD model analysis

Xiaochen Ma [a,*], Wenchao Shi [a], Hongxing Yang [a,*]

[a] Renewable Energy Research Group (RERG), Department of Building Environment and Energy Engineering, The Hong Kong Polytechnic University, Hong Kong, China

Abstract

As a sustainable cooling technology, indirect evaporative cooling (IEC) has been widely recognized as an effective means of achieving carbon neutrality based on its low energy consumption and high efficiency in central air conditioning (AC) systems of buildings. In contrast to the conventional arrangement, IECs as heat recovery units are often arranged in a diamond shape inside the air handling units (AHUs) of data centers (DCs), an approach that facilitates the flexible use of space and integration within the units in a more compact form. The use of CFD simulations allows an integrated analysis of the coupling of hydrodynamic, thermal and mass properties helps to improve the evaporation performance of IECs. In this study, a 3D simulation model of a diamond-shaped IEC containing the water spray system was developed to compare and analyze the air-water arrangement options in IEC systems currently used in DCs, and the corresponding characteristics are explored from the perspective of CFD techniques to determine the effect of nozzle configurations on the formation and evaporation of water film within the wet channels. Then, parametric analysis of nozzle setup schemes based on performance metrics showed that the nozzle arranged in top-side configuration and paired with the air-water counterflow form had the best performance, with 59.2% and 27.4% improvement in water film coverage area and temperature drop, respectively, over the worst scheme (bottom configuration) at a water supply flow rate of 65 L/s. Finally, the effectiveness of the enhanced approach was simulated and analyzed for hydrophilic and fiber coatings, and it was found that the water film coverage increased by 14.5% and 31.6%, respectively, while the coefficient of performance (COP) increased by 7.4% and 16.1%.

Keywords: Indirect evaporative cooler; Data center; Energy recovery; Nozzle configurations; Improvement

* Corresponding authors.
E-mail addresses: xiaochencc.ma@connect.polyu.hk (X. Ma), hong-xing.yang@polyu.edu.hk (H. Yang).

Nomenclature

A	surface area, m^2	*Subscripts*	
C_D	drag coefficient	l	latent
d_e	the diameter of the channel, m	p	primary air
e	specific exergy, J/kg	s	secondary air
f_{Re}	friction coefficient	w	wetted area
g	gravitational acceleration, m/s^2	wh	the whole area of surface
H	height of the nozzle position, mm	th	thermal
i	specific exergy	me	mechanical
k	thermal conductivity, W/(m·K)	ch	chemical
P	pressure, Pa	in	inlet
Q	water flow rate, kg/s	out	outlet
Re_s	Reynolds number		
t	contact time	*Abbreviations*	
u	velocity, m/s	*3D*	Three dimensional
v	kinetic velocity, m/s	*AC*	Air conditioning
W	power, kW	*AHU*	Air handling unit
		CFD	Computational Fluid Dynamics
Greek letters		*COP*	Coefficient of Performance
α	the volume fraction of the phase	*DC*	Data center
β	coverage ratio	*DPM*	Discrete Phase Model
$\bar{\omega}$	longitudinal velocity, m/s	*EWF*	Eulerian Wall Film Model
ρ	density, kg/m^3	*IEC*	Indirect evaporative cooler
μ	dynamic viscosity, kg/(m·s)	*RH*	Relative Humidity
ε_{wb}	wet-bulb efficiency	*RNG*	Renormalization group
η	effectiveness		

1 Introduction

The growth in information demand driven by the Covid-19 pandemic involving global regions and the rapid development of emerging 5G network technologies have led to a surge in demand for cloud-based storage, data transfer and processing services across all industries [1]. Today, data centers (DCs), the places where centralized electronic information equipment is built to operate, have been scaled up at an unprecedented rate. Although the average power usage effectiveness (PUE) value for DCs in Southeast Asia is lower than the global average, the region is experiencing the fastest growth in the DC market[2]. In Hong Kong, the electricity consumption of the DC sector increased by 10.3% in 2019, taking up 4483 TJ and 750 kilotons of carbon dioxide emission [3]. The average PUE of the DC industry in Hong Kong is as high as 2.2 [4], which intensifies the power supply and environmental issues. According to statistics [5], the DC consumes 30-50% of its total energy usage towards cooling to maintain the reliable operations of high-density servers. The cooling solution for DCs in Hong Kong mainly relies on active cooling systems such as Mechanical Vapor Compression Refrigeration (MVCR) which is challenging the climate pledges [6]. Improving the PUE of DCs and reducing carbon emissions with more energy-efficient cooling technologies is therefore essential, especially for areas with limited free cooling resources located in hot and humid climates.

Owing to the high-power consumption of air conditioning (AC) caused by the uninterrupted operation and year-round cooling of DCs, the use of natural cooling resources can help to reduce the burden of DC frequency power supply, achieve long-term business sustainability and improve competitiveness. Indirect evaporative cooling as a widely developed natural cooling technology can transfer heat through the evaporation of water without a compressor thereby reducing the temperature of the medium being cooled [7]. By absorbing the latent heat of vaporization, the secondary air is brought into direct contact with water to complete the isoenthalpy and cool the treated air on the other side of the plate to a lower temperature than itself [8]. Fig. 1 shows the system diagram of a typical IEC for air-conditioning of DC. The water is sprayed into fresh air which is utilized as the secondary air, and the humidity of supply air can be maintained without adding any moisture. The separated channels of fresh air and indoor return air can avoid the cross-contamination to ensure the high levels of cleanness required by DCs. Driven by only a circulation pump and two fans, the IEC provides a promising and sustainable way to extend the period during which DCs can utilize natural cooling resources.

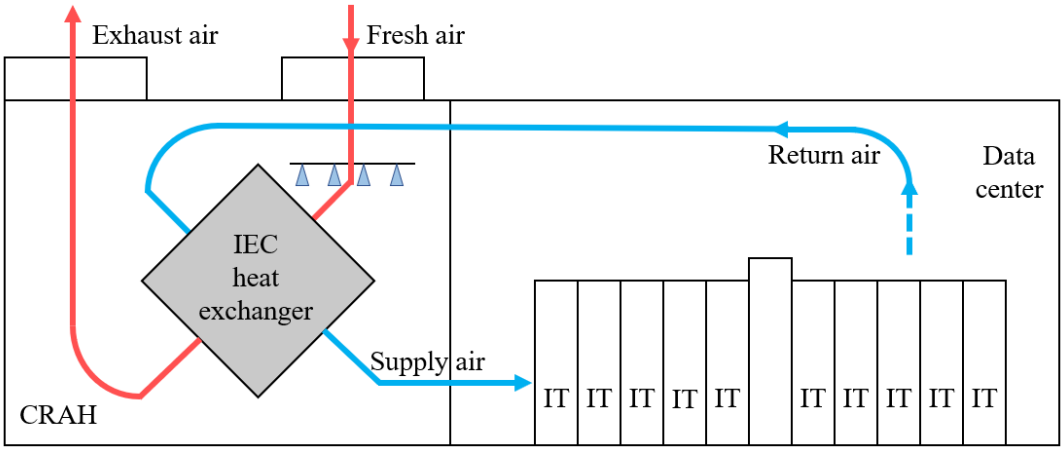

Fig. 1. A typical IEC air-conditioning system of DC [9]

With the unique advantages in lowering PUE and cutting down the carbon footprint, the application of IEC for DCs cooling solution has received worldwide recognition. DigiPlex air-to-air indirect evaporative cooling technology takes advantage of Nordic atmospheric conditions and uses low ambient air temperatures combined with the water spray system to maintain a comfortable thermal environment in the DC. It enables a 30% saving in total power consumption in the DC

compared to the industry average, without loss of quality [10]. This solution can reduce total power consumption by up to one-third by moving from an ordinary DC (PUE of 1.67) to a more energy efficient center (PUE of 1.2) [11]. The German company DencoHappel has developed a unit with a double plate-fin heat exchanger core in series, which extends the flow time of the return air within the core and increases the contact area with the core walls, resulting in improved heat transfer effectiveness for indirect evaporative cooling. The reason why the fresh air does not pass through the condenser after heat exchange is that the cooling capacity carried by the fresh air is already fully utilized inside the core [12]. This plate type double heat exchanger sprayed indirect evaporative natural cooling AC unit is also used in T-block laboratory of Tencent in China, where the PUE tested is less than 1.1, confirming the excellent system energy efficiency [13]. Huawei Linyi, a cloud computing big DC radiating the economic group of southern Shandong and northern Jiangsu, has led the market for cooling solutions for DCs by introducing a new generation of technology that integrates IEC, heat recovery and mechanical cooling in an all-in-one system with an optimized structure. Its application in Linyi Big DC shows an average PUE of 1.25 [14], which is 14% higher than the average value in the same region.

With the widespread adoption of IEC technology in DC, a range of advanced IEC designs have emerged that are more energy efficient. The dew point IEC developed by Maisotenko [15] in 2003 enables the pre-cooling of the secondary air and further reduces the output air temperature around the dew point, and is also called M-cycle. The close proximity to the dew point, the small footprint and the flexibility of the installation form, which can provide output air after wet cooling, are the main research directions for evaporative cooling technology. The National Snow and Ice DC (NSIDC) in Colorado adopted the M-cycle IEC, which resulted in significant energy savings by reducing the PUE from 2.03 to 1.27 compared to traditional refrigeration systems [16]. Excool [17], a British company, has developed a high-pressure spray plate type indirect evaporative cooling AC unit that utilizes physically and chemically treated water atomized at high pressure to increase the contact area between water and outdoor air, enhancing the cooling effect of water evaporation on outdoor air. Besides, for an existing DC in Xinjiang, Guo et al. [18] presented a hybrid system made up of DEC, IEC, and glycol free cooling technology. This system could realize free cooling around the year and a peak yearly energy conservation rate of 73%.

As for the nature of IEC technology, the surface wettability of wet channels has been regarded as a key element that affects the thermodynamic process of water evaporation and the heat removed from the dry side to the wet side. To ensure the surface wettability of wet channels, considerable efforts have been conducted including improvements to wet surface materials and water spray system. The porous materials have been widely applied in evaporative cooling heat exchangers for performance enhancement. A novel regenerative IEC prototype that combined heat pipe and porous ceramic tube sections to the heat exchanger plates was put through testing by Boukhanouf et al. [19]. The measured wet-bulb efficiency of this device is 0.8, and its COP is 11.4. Applying flexible tube nozzles fitted inside the wet channels, Al-Zubaydi et al. assessed the effectiveness of a novel IEC with intermittent water spraying. The mixed mode increased cooling capacity by 25%, according the data [20]. In addition, to clarify the effect of nozzle arrangement above the IEC system water distribution and optimize the water system setup MA et al. proposed a spray distribution model for IEC and studied the optimal centerline distribution scheme. Utilizing this optimized nozzle arrangement scheme, the COP was increased by 16%, which illustrates the significance of a reasonable nozzle arrangement [21]. A numerical model based on heat and mass transfer concepts was developed and verified by Adam et al [22]. The optimal size that provides good efficiency was derived from the findings from simulation results and serves as a guideline for the ideal operating conditions to achieve high operating efficiency. In addition, he investigated distinct condensation

phases in the supply air channel and the effectiveness of the IEC under different phases, highlighting the influence of wettability factors on the condensation state and specifying the circumstances for operation required to achieve high efficiency [23].

Furthermore, two numerical methods frequently used in IEC model setups are the finite difference method (FDM) and the finite volume method (FVM). For FDM models, various models and optimization methods have been developed to predict the performance of IEC systems and to establish the heat and mass transfer progress of IEC, taking into account different factors such as incomplete wetting, inhomogeneous Lewis numbers, water temperature variations, the effect of longitudinal heat transfer and new flow configurations [24,25,26,27]. Although exceptional simulation results could be provided by the FDM model in a reasonable time frame, it can be challenging to deal with 3D complexity and more complex hydraulic and thermal properties. On the other hand, CFD, on which FVM is based, is a complex fluid analysis technique that can effectively investigate the full range of thermal and mass transport processes by figuring out continuity, momentum, energy, and species formulations and exploiting the rapidly evolving capabilities of computer technology [28,29,30]. Table 1 briefly summarizes the comparison of existing models with the present model, and it can be seen that for IEC, there is still a lack of convincing simulation models of water spray systems to consider atomized droplets and the film formed on the channel surface.

Table 1 IEC model with FVM approach

Research	Dimensions	Workbench	Characteristics
Ren et al. [30]	3D	ANSYS FLUENT	Temperature, pressure, average Nusselt and Sherwood number distributions, as well as other variables, were examined using CFD models of the 3D heat and mass transfer process in a plate-type IEC.
Cui et al. [31]	3D	ANSYS FLUENT	It was explained how a DPIEC is affected by the size of the channel, the presence of physical ribs across the channel, and the use of return air as working air. The wet surface was treated as equally dispersed droplets rather than as a thin water coating.
Xu et al. [32]	3D	ANSYS FLUENT	The CFD environment was used to mimic IEC that removed supporting guides. This cooler with unusual efficiency was substantially higher than that of the standard cooler, allowing the IEC size and starting cost to be reduced.
You et al. [33]	3D	ANSYS FLUENT	The use of IEC with heat recovery from cool interior air was investigated. This model was able to forecast the effects of condensation given the local meteorological conditions.
Wan et al. [34]	3D	COMSOL	Several inlet air characteristics were developed into empirical formulae for the heat and mass transfer coefficient in tropical climates.
Shi et al. [35]	3D	COMSOL	Investigations were made on the steady-state non-uniformity distributions of temperature and humidity across the channel y-direction. The effects of the geometric parameters and inlet supply air characteristics were evaluated.

This research	3D	ANSYS FLUENT	The water spray system with falling film was combined in the model for the diamond-shaped IEC. The coupling of hydrodynamic, thermal and mass properties of each sector were explored. The nozzle configurations were optimized, and energy-saving performance was assessed.

Finally, based on the advantages of IEC technology as a green and sustainable cooling strategy, there is still a huge potential for optimization in its application in DCs. Firstly, the critical heat generation of servers requires large cooling systems with extremely high cooling capacity. As a result, large heat exchangers are required for IECs in DCs to handle the critical heat generation of servers, which increases the challenge of achieving sufficient surface wetting over the entire plate surface [36]. Secondly, large evaporative cooling units in DC systems usually result in high water supply rates and thus increased pump power. In addition, continuous water circulation at high flow rates may increase the risk of leakage and deteriorate the performance of the system. Therefore, a coupled model of the water spray system and water film distribution for a diamond-shaped IEC is developed to investigate the comprehensive effects of nozzle settings and airflow configurations on the wettability of the IEC surface. Ultimately, the optimal nozzle setting is targeted and the improvement in energy efficiency is further clarified in conjunction with functional coating optimization measures.

2 Methodology

2.1 Working principal of IECs

The IEC unit is composed of a plurality of completely isolated dry and wet channels for the primary and secondary airflows respectively. When the IEC system is running continuously, the nozzles located at the top would spray water droplets into the wet channels, thus forming the water membrane on the wall surface. Then the secondary air makes contact with the attached water membrane, the surface of the plate is cooled by the evaporation phenomenon that removes some of the latent heat. Meanwhile, the primary air from the adjacent dry channels gets in touch with the surface of the cold plate to achieve the cooling effect. During this period, the supply air can be cooled in the dry channel without direct contact with water, thus achieving cooling in isohygroscopic conditions. Fig. 2 exemplifies the enthalpy as well as humidity diagram of the IEC auxiliary air conditioner, where the primary air in the dry channel undergoes an equal enthalpy cooling process and the secondary air experiences a both cooling and humidification process. Therefore, the secondary air completes isoenthalpic cooling from state point 1 to state point 4, which is approximated as an adiabatic process. Meanwhile, the heat from the drying channel is transferred to the secondary channel and the water at state point 4 continues to warm up and evaporate faster, eventually reaching state point 3 [37].

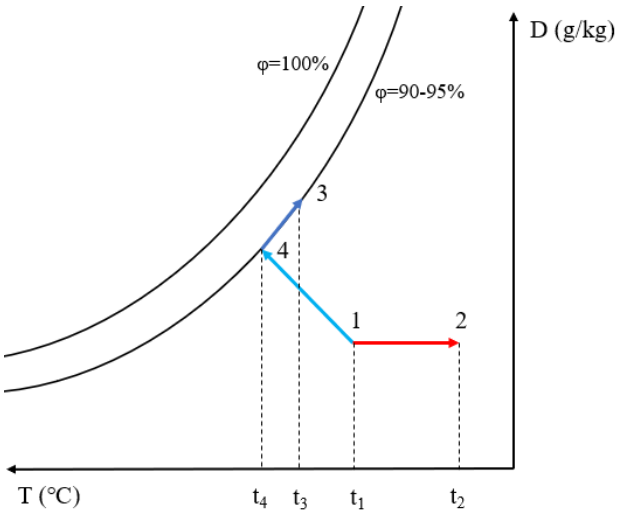

Fig. 2. The psychrometric chart for IEC

2.2 Description of the model geometry

Different from the conventional IEC placement (Fig. 3 (a)), IECs which installed as a heat recovery unit in the AHU of DCs are often distributed in a diamond shape due to their compactness and flexible arrangement, as exemplified in Fig. 3 (b). The baseline model was set up in the Space claim unit embedded in the ANSYS work bench, and the coverage factor of the water film on the surface of the wet channel will be taken into consideration as a major research aspect in this study. For focused investigation, the model will be built assuming that the properties of water and air are constant with the incompressible element and the plate of the IEC is adiabatic [38].

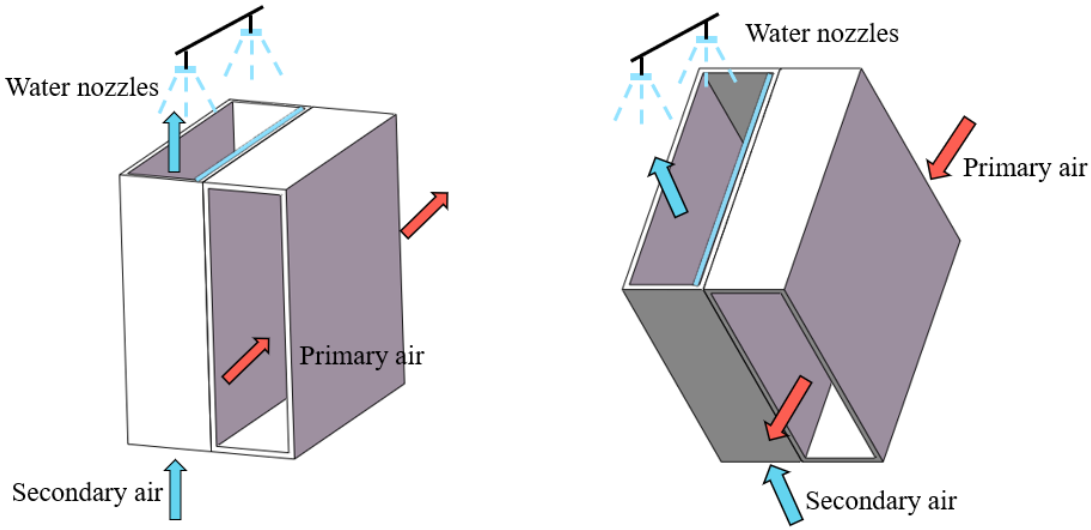

(a) Conventional IEC (b) Diamond-shaped IEC

Fig.3. Two types of IEC models set up in work bench

2.3 Mathematical bases of CFD approach

The following is a list of the control three types of conservation equations for momentum, mass conservation and energy respectively.

$$\frac{\partial}{\partial t}(\rho E) + \nabla \cdot (\rho u^2) = -\nabla P + \nabla \cdot \left(\mu\left(\nabla u + \nabla u^T\right)\right) + \rho g + F \quad (1)$$

$$\frac{\partial}{\partial t}(\rho) + \nabla \cdot (\rho u) = 0 \quad (2)$$

$$\nabla \cdot \sum_{k=1}^{n} \left(\alpha_k v_k (\rho_k E_k + p)\right) = \nabla \cdot (k_{eff} \nabla T) + S_E \tag{3}$$

For the selection of turbulence mode, the Reynolds number of the air treated in this investigation was the range of 5,000-13,000 with the water film less than 400. Therefore, the flow form of the falling water film and treated air were laminar and turbulent respectively. Based on the reference of Fluent user's guide [39], RNG (Renormalization group) turbulence model was chosen to simulate the behavior of the fluid dynamics in the IEC. The controlling equations for the turbulent kinetic energy as well as its dissipation rate could be determined as follows.

$$\frac{\partial}{\partial t}(\rho k) + \frac{\partial}{\partial x_i} \cdot (\rho k u) = \frac{\partial}{\partial x_j} \cdot \left(\alpha_k \mu_{eff} \frac{\partial k}{\partial x_j}\right) + G_k + G_b - \rho\varepsilon - Y_M + S_k \tag{4}$$

$$\frac{\partial}{\partial t}(\rho \varepsilon) + \frac{\partial}{\partial x_i} \cdot (\rho \varepsilon u_i) = \frac{\partial}{\partial x_j} \cdot \left(\alpha_\varepsilon \mu_{eff} \frac{\partial \varepsilon}{\partial x_j}\right) + C_{1\varepsilon} \frac{\varepsilon}{k} \cdot (G_k + C_{3\varepsilon} G_b) - C_{2\varepsilon} \rho \frac{\varepsilon}{k} - R_\varepsilon + S_\varepsilon \tag{5}$$

Owing to the presence of evaporation in the wet channel of IEC, the phase change process produces a degree of heat and mass transfer, hence the simulation needs to incorporate the species transfer model formulated by Eq. (6). For the species transport, the description are as follows.

$$\frac{\partial}{\partial t}\left(\alpha_q \rho_q x_{k,q}\right) + \nabla \cdot \left(\alpha_q \rho_q \vec{u} x_{k,q} - \alpha_q D_{k,q} \nabla x_{k,q}\right) = S_{lg,k} \tag{6}$$

The Volume of Fluid (VOF) model, which is originally the most widely used falling film interface capture model has undergone a series of refinements and has matured since its development [40]. The description equation for the volume fraction could be shown in Eq. (7).

$$\frac{\partial \alpha_{1/g}}{\partial t} + \vec{u} \cdot \nabla \alpha_{1/g} = 0 \tag{7}$$

Based on solving Eq. (7) to acquire the volume fraction within each involved section, Eqs (8), (9) and (10) illustrate that the associated thermal characteristics could also be determined.

$$\rho = \alpha_1 \rho_1 + \alpha_g \rho_g \tag{8}$$

$$\mu = \alpha_1 \mu_1 + \alpha_g \mu_g \tag{9}$$

$$\lambda = \alpha_1 \lambda_1 + \alpha_g \lambda_g \tag{10}$$

The DPM (Discrete Phase Model) will be used to simulate the operating status of the nozzles in the IEC water system, including the trajectory of the spray droplets from being ejected, to falling into the wet channel, to finally colliding with the wall or leaving the wet channel.

The trajectory of droplets can be determined based on a combined Euler-Lagrangian method by solving the force balance equation written as Eq. (11).

$$\frac{d\left(\overrightarrow{X_g}\right)}{dt} = \overrightarrow{V_g} \tag{11}$$

The movement description of a single droplet is described by Eq. (12).

$$\frac{d\left(m_d \overrightarrow{F_d}\right)}{dt} = \overrightarrow{F_D} + \overrightarrow{F_g} \tag{12}$$

For a circular drop, the drag force formulated by Eq. (13).

$$\vec{F}_d = -\frac{\pi}{8} C_D \rho_a D_d^2 \vec{V}_r \left|\vec{V}_r\right| \tag{13}$$

The EWF (Eulerian Wall Film) model could be used to describe the process by which water droplets in contact with the wet channel wall are trapped by the plate to form a thin water film attached to the plate and flow down the plate, following the relationship of Eqs. (14) and (15).

$$\frac{\partial \delta}{\partial t} + \nabla \cdot (\delta u_l) = \frac{\dot{m}_s}{\rho_l} \tag{14}$$

$$\dot{m}_s = \alpha_l \rho_l u_{l,n} \tag{15}$$

Finally, interfacial mass transfer also needs to be considered due to the phase change reaction resulting from the evaporation of the liquid in the wet channel. In this process, the local mass transfer coefficients as well as the total mass transfer coefficients are reflected by Eqs. (16), (17) and (18), respectively.

$$h_{m,g} = 2\sqrt{\frac{D_g}{\pi t_c}} \tag{16}$$

$$h_{m,l} = 2\sqrt{\frac{D_l}{\pi t_c}} \tag{17}$$

$$\frac{1}{K} = \frac{1}{h_{m,g}} + \frac{1}{\psi h_{m,l}} \tag{18}$$

Based on the total mass transfer factor K, the mass source component and the energy component at the phase surface could be determined by Eqs. (19) and (20).

$$S_{lg,k} = K\,(d_g - d_e)\,A \tag{19}$$

$$S_E = \sum_{k=0}^{m-1} S_{lg,k}\, H_{lg,k} \tag{20}$$

2.4 Simulation settings

The schematic diagram of IEC and computational domains are illustrated in Fig. 4. The whole model is consisting of two domains to describe the direction and state of gas-liquid flow in the dry and wet channels respectively. The finite control volume method could be applied to deal with the control equations. Since gravity is not negligible, the weight-pressure discretization method is used [41]. The SIMPLE method is applied for the pressure-velocity coupling and then the pressure interpolation technique (PRESTO!) is used [42]. In the calculation domain for the wet channel, the inlet and outlet of the secondary airflow are at a certain distance compared to the heat exchanger prototype, allowing the nozzle model, which is located inside the external boundary of the heat exchanger, to deliver a smooth spray into the wet channel. Therefore, the continuously fed spray makes contact with the plate surface and forms a continuous film of water flowing along the wall lead by gravity. The wet air flows beside the water film in a downstream, counterflow or staggered flow. Since the differential temperature between the water membrane and the secondary air flow, heat absorption by evaporation of the liquid occurs in the channel. The entire channel is the computational domain of the cross-flow because of the asymmetry of the air flow and the water flow. On the other hand, for the computational domain of the dry channel, the primary airflow enters from the upper right and condensation occurs when the humidity is too high, then the airflow undergoes cooling and dehumidification before leaving the dry channel from the lower left. The dimensions of all calculation domains are 620 × 620 mm (L × H). As shown in Fig. 4, the grid size in the area close to the plate surface should be fine enough in order to ensure a correct interface description. The mesh size in the interface region is less than 0.1 mm.

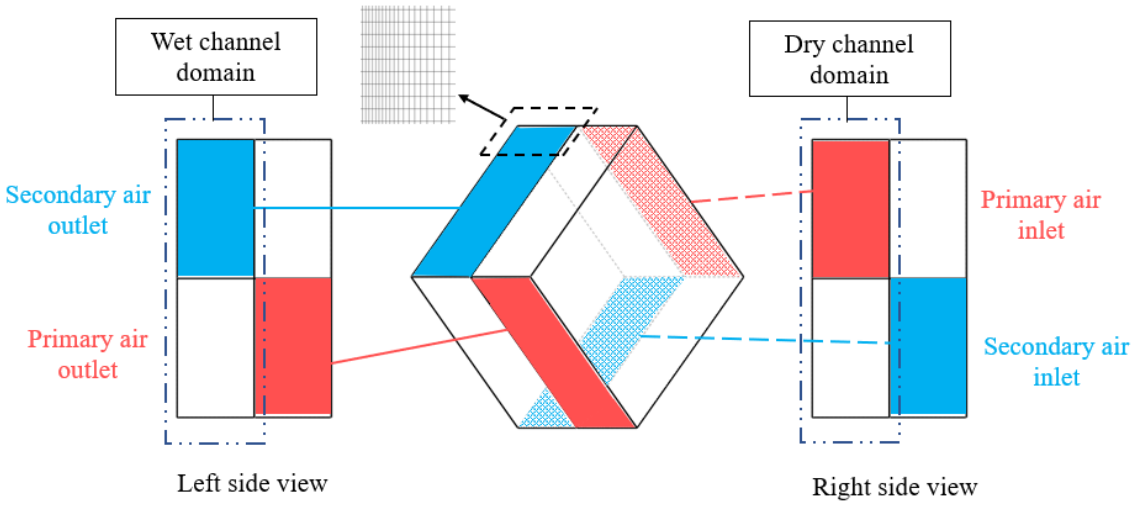

Fig. 4. Geometry, mesh and boundary conditions in simulations

2.5 Grid independence verification

To complete the simulation of the mathematical model, the base model created in Space claim needs to be meshed. As the key point of this study is the water membrane that forms on the plate surface when the spray droplets come into contact with the wet channel, the film is quite thin and flows slowly down the wall surface by gravity. To accurately obtain the distribution of the film on the surface and the flow characteristics, a fine size grid with a size of less than 0.1 mm was selected in the area close to the plate surface. It is well known that the results of the model calculations will be closer to the true value due to the increase in the number of meshes, and the mesh quality is higher while the time cost of the program to run the calculation is also higher. Therefore, a reasonable balance between mesh quality and computational time is required, and grid independence is verified to select the number of meshes that are close enough to the exact value. For the air side, the velocity of inlet primary air was set at 3.7 m/s, the absolute humidity was set at 10 g/kg, and the temperature was determined as 35°C. For the water side, the water supply flow rate was selected to be 65 L/h. Fig. 5 compares the water membrane coverage factor on the wet channel wall and the primary air output temperature for different grid quantities. It is clear that both evaluation parameters initially deviate significantly with the grid mass and then level off at a grid number of 450,000. Thus, this grid structure was selected for further simulations so as to maintain a balance between simulation accuracy and processing time.

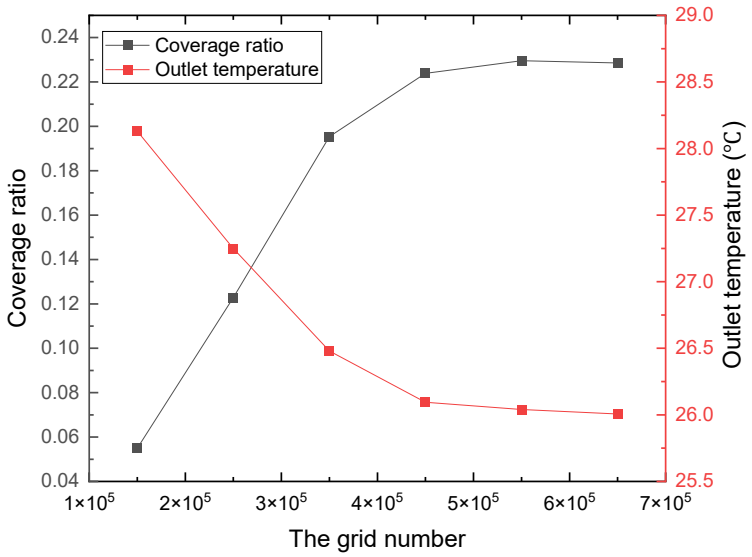

Fig. 5. Coverage ratio and outlet temperature at different accounts of grid

2.6 Description of performance evaluation indicators

The water film coverage factor of the wet channel walls is considered as one of the important components influencing the evaporation phenomenon as a valid reference for assessing nozzle settings and is calculated as the ratio of wetted area to entire area, written as Eq. (21).

$$\beta = \frac{A_w}{A_{wh}} \tag{21}$$

The wet-bulb efficiency is selected for assessing the capacity of the IEC for handling sensible heat. It is a metric used to quantify how closely the wet-bulb temperature of the secondary air coming the channels at the inlet approaches the outflow primary air temperature, which is shown by the equation Eq. (22) [43].

$$\varepsilon_{wb} = \frac{t_{p,in} - t_{p,out}}{t_{p,in} - t_{wb,s}} \tag{22}$$

By utilized the fresh air to pre-cool the supply air, the IEC lowers the cooling burden on the mechanical cooling system. The extra power demands of the selected pre-treatment system, as well as the power utilized by the cooler for conventional cooling and dehumidification of the supply air, should be included in the entire energy consuming of the AC system coupled to the IEC. On the basis of several basic definitions and descriptions of items, and applying the empirical equations of Shi et al., the following equations can be used to figure out the energy consumption of an IEC [44, 45].

The energy demand of the fan is strongly influenced by the pressure drop, so it is essential to first determine the pressure drop and then the total energy demand of the fan could be identified by hydraulic calculation as follows:

$$f_{Re} = 96 * (1 - 1.3553(\frac{L}{s}) + 1.9467\left(\frac{L}{s}\right)^2 - 1.7012\left(\frac{L}{s}\right)^3 + 0.9564\left(\frac{L}{s}\right)^4 - 0.2537\left(\frac{L}{s}\right)^5) \tag{23}$$

$$d_e = \frac{2sL}{s+L} \tag{24}$$

$$\triangle P = \frac{f_{Re}L\rho u^2}{2Red_e} \tag{25}$$

$$W_{fan} = \frac{Q \triangle P}{3600 \times 1000 \times \eta_0 \times \eta_1} \times K \tag{26}$$

The energy consumption of pumps, another component of IEC energy requirement, is usually calculated based on a combination of gravity, height differences of nozzles and valves and the total water supply flow:

$$W_{pump} = m_w g\left(h_{gravity} + h_{nozzles} + h_{valves}\right) \times K \tag{27}$$

The COP value reflects the energy efficiency of cooling for different nozzle configurations by measuring the relative proportion of the cooling capacity provided by the IEC to the entire energy consuming of the system, and the determined formula is [46]:

$$Q_p = m_p c_{pg}\left(t_{p,in} - t_{p,out}\right) \tag{28}$$

$$COP = \frac{Q_p}{W_{fan} + W_{pump}} \tag{29}$$

2.7 Description of exergy analysis

The determination of dead state conditions is significant for exergy analysis. A constant atmospheric condition is frequently used as the benchmark environment [47]. Nevertheless, there is still exergy accessible when the atmosphere is not completely filled with air. Water would be able to spontaneously disperse into the unsaturated air and finally achieve saturation through such a moist air process. As a result, the dead state in this essay is referred to as saturated outside air.

The exergy used to reach thermal, mechanical and chemical equilibrium with the atmosphere during indirect evaporative cooling process can be written as [48]:

$$e_t = e_{th} + e_{me} + e_{ch} \tag{30}$$

The combination of dry air and water vapor found in humid air makes it an ideal gas. The following equation was developed by Wepfer et al. to represent the entire flow exergy of moist air per kilogram of dry air [47]:

$$Ex_a = \left(C_{P,DA} + \omega C_{P,V}\right)\left[T - T_0\left(1 - \ln\frac{T}{T_0}\right)\right] + T_a\left[(1 + 1.608\omega)\ln\left(\frac{1 + 1.608\omega_0}{1 + 1.608\omega}\right) + 1.608\omega\ln\frac{\omega}{\omega_0}\right] \tag{31}$$

The exergy balance for the basic heat exchanger is shown in Fig. 6. As there is no work being produced for the reaction process of IEC system, the exergy balance for the IEC is determined as follows [49]:

$$\left(m_i e_{1,a} + m_{w,i} e_{w,a}\right) = \left(m_f e_{2,a} + m_3 e_{3,a}\right) + I \tag{32}$$

Consequently, the exergy efficiency of the IEC is depicted as:

$$\eta_e = 1 - \frac{I}{\left(m_i e_{1,a} + m_{w,i} e_{w,i}\right)} \tag{33}$$

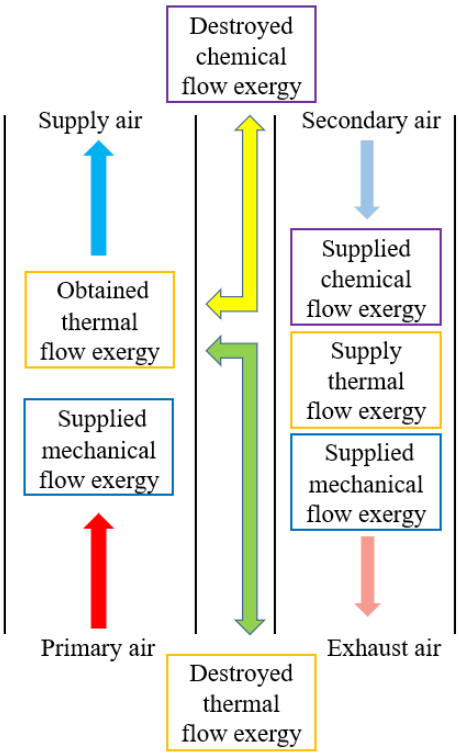

Fig. 6. The schematic diagram of exergy analysis

3 Model validation

3.1 Validation of the water spray system

The accuracy of the CFD model developed in this research for a diamond-shaped IEC is verified based on a comparison and analysis of the simulation data with the field trial data in the literature by De Antonellis et al [50]. In the experiments, the fluctuation of the wet-bulb efficiency of the diamond-shaped IEC (TOP/SIDE configuration) was investigated when the water spray flow rate was varied. The temperature drops at the supply air outlet compared to the inlet at different flow rates was compared under the fixed inlet air characteristics, heat exchanger geometry and heat transfer coefficients provided in the literature. According to Fig. 7, the trend of primary airflow temperature drop with water supply flow is the same in both sets of data, and the maximum difference is less than 10%, hence the CFD model fits the water system and temperature drop to the required degree.

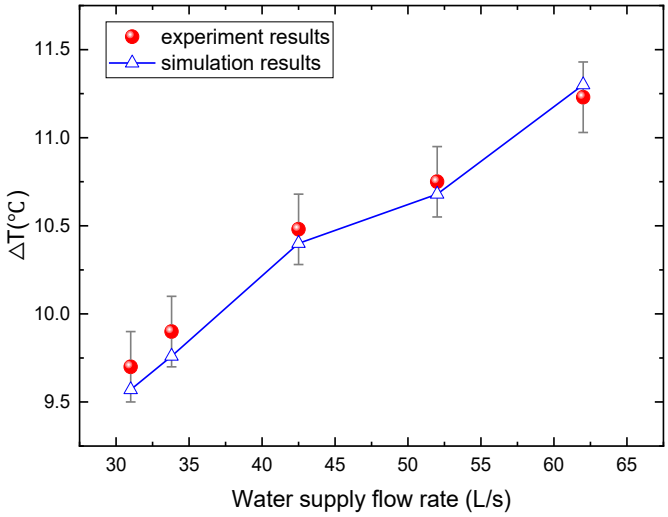

Fig. 7. Comparison between the tested and simulated data based on temperature difference

3.2 Validation of Film thickness

As was noted in section 2.3, the main form of downward flow of the water film formed by the aggregation of liquid droplets inside the IEC wet pass due to gravity is wavy laminar flow. The average membrane thickness of the Nusselt-based liquid film theoretical laminar flow could be determined by the analytical equation of the film, as shown in the following equation [51],

$$\delta_w = \left(\frac{3\nu_w Re_w}{g}\right)^{1/3} \tag{34}$$

This section compares the average membrane thickness values derived from this simulation model with the estimated results of the preceding analytical equation, and the outcomes are displayed in Fig. 8, with the purpose of confirming the accuracy of the suggested CFD model in terms of flow. It is obvious that the simulated results and the estimated outcomes of the empirical equation correspond well. Therefore, it is accurate to simulate the water film flow formation in the IEC wet channel using the current model.

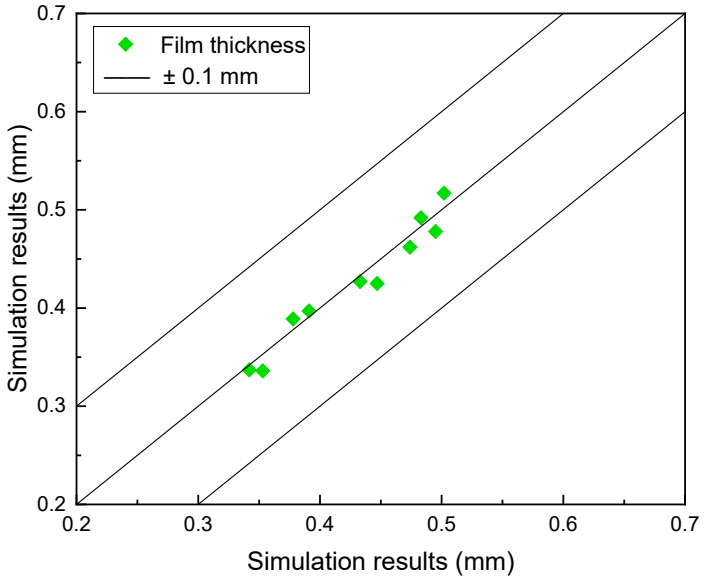

Fig. 8 Validation of film thickness between simulation results and Nusselt empirical formula

3.2 Validation of IEC system

To gain a fuller understanding of the precision of the model in foretelling the performance of the overall IEC system, tested data from an IEC combined with AHUs set up at a printing facility in Hong Kong was also considered for validating. In this project, the IEC was made of aluminum sheets with a thickness of 0.5 mm, and a total of 90 channel pairs of fresh air and return air were placed in a width of 0.8 m space. By referring to the fresh air demand of 3312 m^3/h, the area of each heat exchange plate is designed as 0.384m^2 with a dimension of 0.62 m × 0.62 m. The total heat exchanger area of this IEC is 69.1 m^2.

To collect the operation and performance data of the IEC system for performance analysis, a data monitoring system. A variety of kinds of senders are required to transmit real-time measured data to a data logger and Table 2 lists the specific parameters of these instruments. The data measured by these transmitters was collected in every 5 minutes.

Table 2 Specifications of the test parameters

Sensor	Parameter	Range	Accuracy
T&R Transmitters	Temperature,	-10-60 ℃	± 0.25% ℃
	Humidity	-15-95% RH	± 2.0% RH
ΔP Transmitters	Air velocity	0-15 m/s	± 1%

With the purpose of identify the reliability of the test results, the uncertainty introduced by the errors of the quantified instruments used during the experiment needs to be analyzed. The method Eqs. (35) and (36) for calculating the uncertainty of the measurement equipment and the experimental factors according to the error analysis guidelines provide how to calculate the uncertainty of the measurement equipment and the experimental factors respectively [52, 53].

$$U = f(x_1, x_2, x_3, \dots, x_n) \tag{35}$$

$$\delta U = \sqrt{\left(\frac{\delta U}{\delta x_1}\delta x_1\right)^2 + \left(\frac{\delta U}{\delta x_2}\delta x_2\right)^2 + \left(\frac{\delta U}{\delta x_3}\delta x_3\right)^2 + \cdots + \left(\frac{\delta U}{\delta x_n}\delta x_n\right)^2} \quad (36)$$

On the account of the accuracy data of each testing equipment arranged in Table 1, the uncertainty of the wet-bulb efficiency by the experimental assessment criteria is 2.47%.

The initial parameters of field test were applied in the simulation model as well. The experiments were conducted under the following conditions: $t_p = 35$ ℃, $RH_p = 50\%$, $u_p = 2\ m/s$, $t_s = 24$ ℃, $RH_s = 60\%$, $u_s = 1.5\ m/s$, $s = 4\ mm$, $H = 0.5m$, $L = 0.5\ m$. Fig. 9 reflects the comparison of the simulated results of wet bulb efficiency with the experimental results, and according to the results it was found that the deviations of these points are within 10%, and the maximum difference is 8.6%, Consequently, the proposed CFD model is proved acceptable for subsequent research.

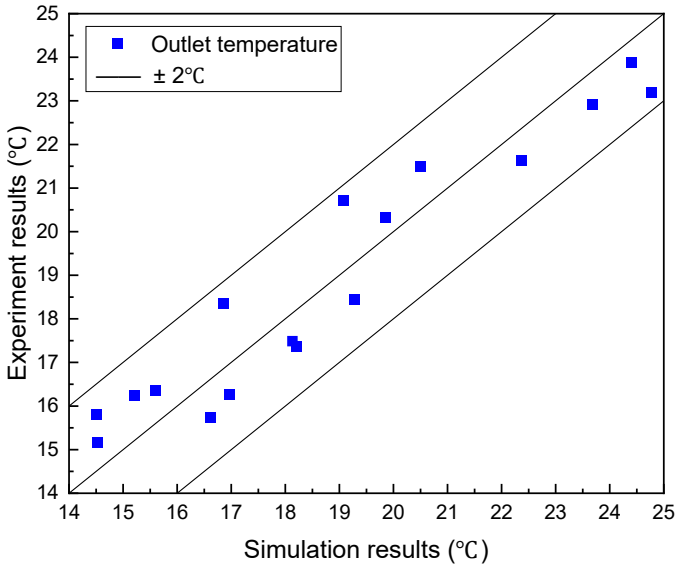

Fig. 9. The model verification results based on the outlet temperature of primary airflow

4 Effects of nozzle configuration on cooling characteristics

To improve the performance of the IEC as a heat recovery unit for AHUs in DCs and determine the optimal nozzle design for the diamond-shaped IEC, this section presents a comprehensive CFD analysis of the air-water configuration, including the installation position of the nozzles and the direction of the airflow relative to the water flow.

4.1 Four schemes of nozzle configuration

On the basis of the literature summaries and surveys of actual AHU heat recovery devices in DCs with taking into account the installation space with flexible arrangement of IECs, the common nozzle setting configurations can be summarized into the four types illustrate in Fig. 10, namely upper side configuration, lower side configuration, top configuration and bottom configuration. Moreover, previous studies on the heat and mass transfer of IECs have demonstrated that the counterflow configuration results in stronger evaporative response in the wet channel compared to the co-current flow configuration. This is because the secondary air and water streams in the wet channel are in contact with water more fully and for a longer period of time in the counterflow case. Therefore, this

section analyzed the performance of four nozzle configuration options founded on the premise of air-water reverse flow, and the superior option would be determined through systematic analysis.

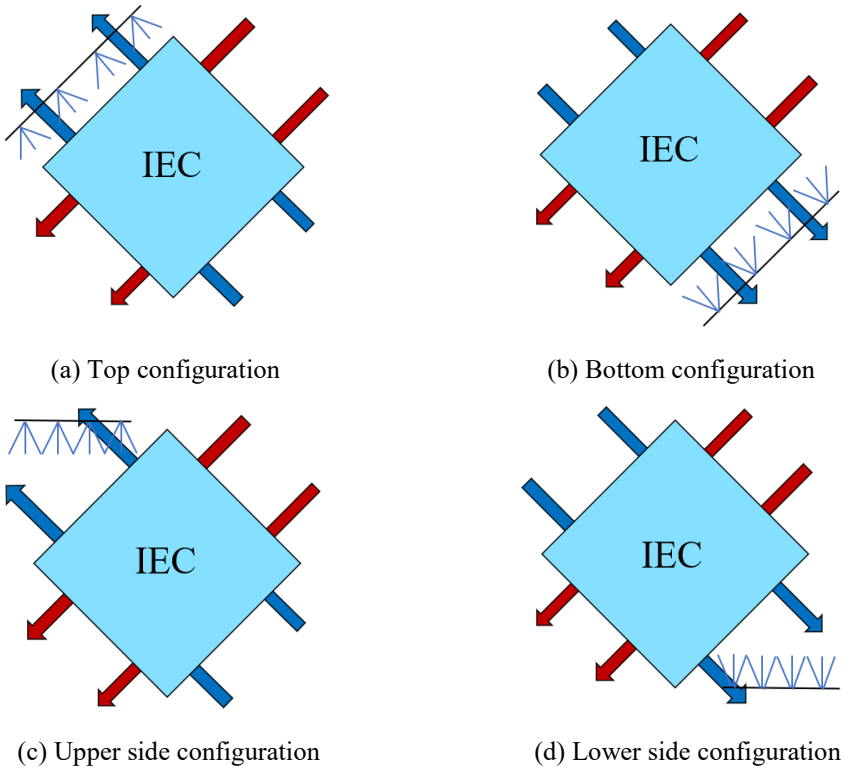

(a) Top configuration (b) Bottom configuration

(c) Upper side configuration (d) Lower side configuration

Fig. 10. The schematics of the four nozzle configurations

4.2 Performance evaluation of different nozzle configurations

4.2.1 Determination of the nozzle parameters

In advance of comparing different nozzle system setup scenarios, the water supply flow rate should be determined when the water film attached to the wetted channel wall tends to be at the maximum wetting ratio. According to the experimental data of De Antonellis et al., the trend of IEC wet-bulb efficiency with water supply flow rate can be derived as shown in Fig. 11 [54]. In general, the wet -bulb efficiency of diamond-shaped IEC usually grows with the increase of water supply flow rate and stabilizes at a maximum value when the flow rate arrives 65 L/s, thus 65 L/s is determined as the simulated flow rate value.

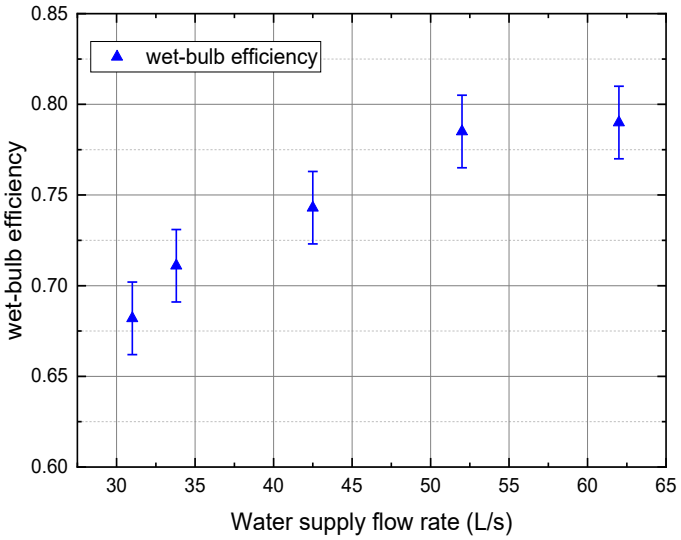

Fig. 11. The determination of test spray flow rate [54]

Besides, with reference to the previous study on the uniformity of spray distribution, a full cone nozzle with an outlet diameter of 2.4 mm was used as the subject of this paper on the water film coverage [21]. Similarly, since this type of nozzle achieves the most ideal spray distribution at a spray cone angle of 45°, this operating parameter is also applied in the simulation of this research. In addition, according to the actual design instructions and previous studies have proven that the nozzle flow rate, pressure, droplet diameter and spray cone angle are interrelated factors. The main characteristic equations of the nozzle are as follows. According to Lefebvre and McDonell, the theoretical parameters of spray can be calculated as Equation (37), (38) and (39) [55].

$$\dot{m}_{th} = \rho A_O \left(\frac{2\Delta P}{\rho}\right)^{0.5} \tag{37}$$

$$d = 9.5 d_j / \left(\Delta P_1 sin(\alpha/2)\right) \tag{38}$$

$$2\alpha = 334.32 K^{-0.165} \left(\frac{D_S}{D_O}\right)^{-0.484} W_e^{0.043} Re_p^{-0.065} \tag{39}$$

Therefore, it is clear that after the spray cone angle and flow rate are determined, the remaining parameters can be specified as shown in Table 3. Water supply temperature that is the temperature of liquid water at room temperature 20°.

Table 3 The specifications of the nozzle

Nozzle type	Orifice diameter (mm)	Volumetric flow Rate (L/s)	Pressure (bar)	Spray angle (°)	Water temperature (℃)
Full cone	2.4	220	1.5	45	20

Finally, for the smooth operation of the wet channel simulation and the subsequent further comparison of IEC performance, the air and water conditions of the IEC need to be identified first, with the following parameter conditions:

$t_p = 35$ ℃, $RH_p = 50\%$, $u_p = 2\ m/s$, $t_s = 24$ ℃, $RH_s = 60\%$, $u_s = 1.5\ m/s$, $s = 4\ mm$, $H = 0.5m$, $L = 0.5\ m$

4.2.2 Comparison of four configurations on water film coverage

Fig. 12 depicts the simulated water film coverage levels within the IEC wet channel for each of the four scenarios with different nozzle configurations.

For the horizontal configurations (top and bottom), the distribution pattern of the water membrane in the wet channel is similar to that of the conventional IEC (square), with minor differences due to the direction of the secondary air flow since a change from the conventional reverse flow to a 45° direction of flow. Furthermore, on account of the characteristics of the diamond-shaped IEC under study, the horizontal configuration, although providing a good flow of water film, concentrates the water film more on the side with the position of nozzles installation, while the plate surface near the primary airflow outlet is not sufficiently wetted. This disadvantage is even more serious in the bottom configuration of the nozzle scheme. As a result of the inevitable gravitational forces, the nozzles need to be set at a higher water pressure in order to deliver the spray droplets into the upper part of the wet channel. However, when the spray pressure is too high, the droplets tend to atomize making it difficult to form a water film in contact with the walls. Therefore, for the lower configuration, the water film is not uniformly distributed in the upper left side of the diamond-shaped IEC, and is subject to the gravity factor even if the right side of the heat exchanger where the nozzle is set is not sufficiently wetted.

For the side configuration of the nozzle, IEC wet channel wall water film distribution of uniformity and coverage compared to the forward configuration is better, whether the nozzle with upper or lower installation. In the case of nozzle for the side on the configuration, the overall distribution of water film tends to spray direction, that is, 45°. At the same time, the water film is affected by gravity and slips along the vertical direction when it comes in contact with the wall, thus the water film is more uniformly distributed and covers a wider area. Likewise, as a consequence of the direction of the nozzle spray, the upper right side of the wet channel is also mostly covered by the water membrane. In contrast, the lower side of the nozzle configuration produces a narrower water film. However, again, due to the direction of the water spray, the comprehensive water film distribution performance is still better than the vertical installation of the nozzle in the case of downward flow of the water film.

(a) Top configuration (b) Bottom configuration

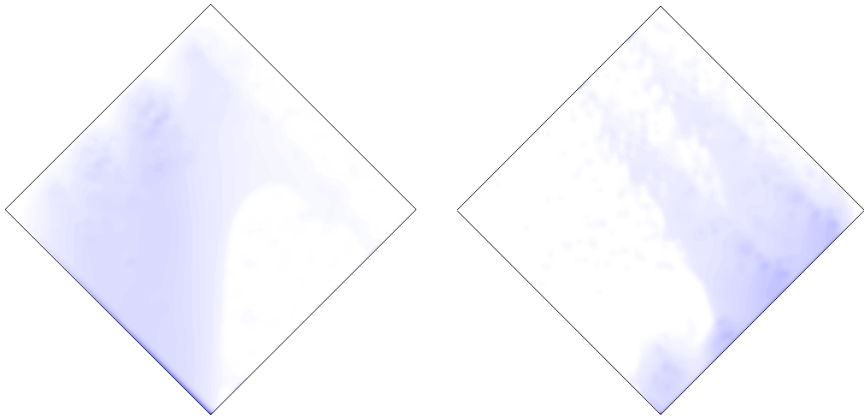

(c) Upper side configuration (d) Lower side configuration

Fig. 12. The water film distribution of the four nozzle configurations

4.2.3 Comparison of four configurations of temperature distribution

Fig. 13 illustrates the temperature distribution states within the IEC primary airflow channel for four different nozzle configuration schemes. It is clear that the degree of temperature drop in the primary airflow temperature within the dry channel is closely related to the percentage of water film coverage within the wet channel. Among them, the IEC with nozzles in the upper side configuration can achieve the minimum outlet temperature of the primary air, and the magnitude of temperature will be significantly more intense and compact inside the heat exchanger channel. This is due to the most intense evaporation process inside the wet channel and the most pronounced cooling effect of the heat exchanger plate, with the primary air being correspondingly more fully cooled in the dry channel. Conversely, the nozzles in the bottom configuration have the worst temperature drop for the same environment and energy consumption due to the most inferior wetting rate.

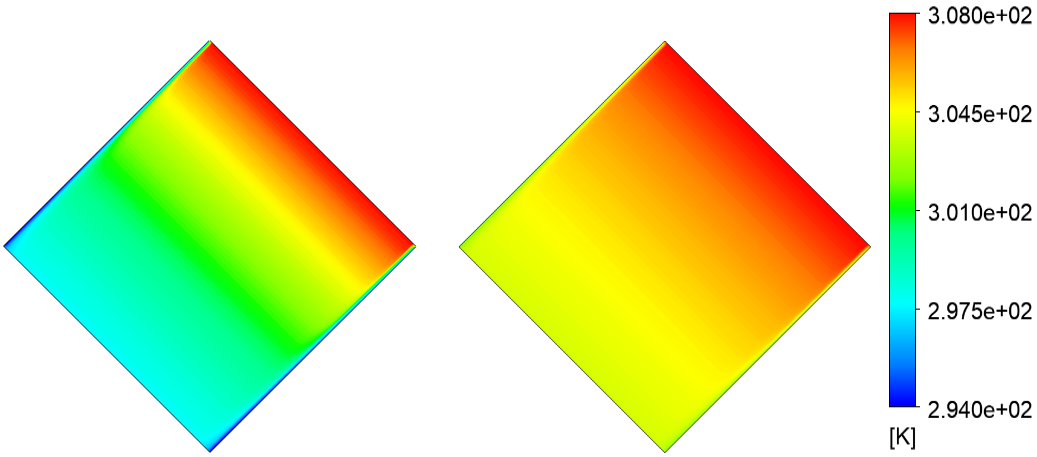

(a) Top configuration (b) Bottom configuration

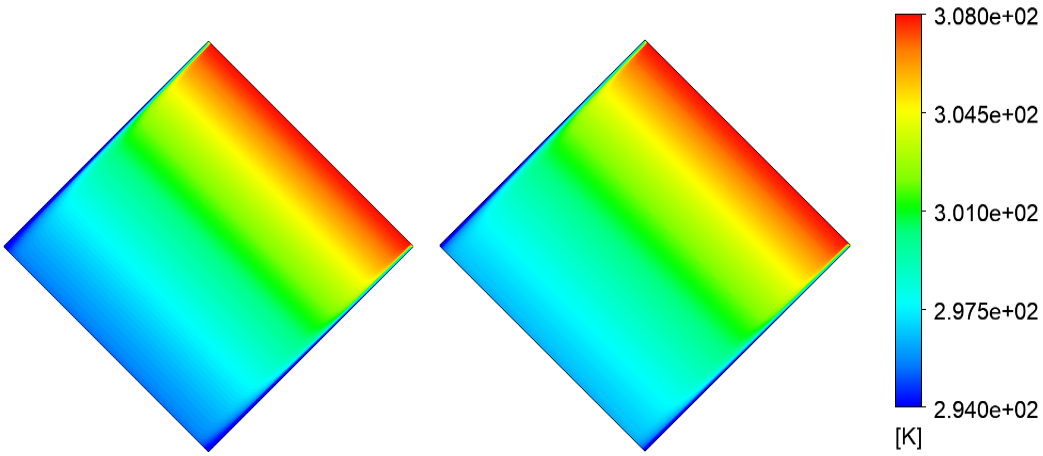

(c) Upper side configuration (d) Lower side configuration

Fig. 13. The primary temperature distribution of the four nozzle configurations

4.2.4 Comparison of configurations of axial characteristics

On the basis of the relative flow directions of the water film and the airflow, the four nozzle configurations could be grouped into two main categories, respectively, the upper and lower spray forms. Therefore, in this section, the upper and lower side configurations are selected as representatives for the water flow and temperature distribution on the plate surface in the thickness direction. The results of this model are allowed to investigate the state of water film formation and the effect of heat mass exchange within the wet channel, as depicted in Fig. 14. Surface tension, gravity and viscous forces all contribute to the flow of the water film. In the initial stage, the water film forms higher thickness in the upper part of the channel section due to surface tension and viscous forces. Due to gravity, the velocity of the water film increases, resulting in the formation of a continuous film on the surface of plate. In addition to the uniform basic characteristics of water film formation, it is clear that by comparing the results of water film distribution between the two water distribution methods that the installation position of the nozzle affects the state of the film formed. In this case, the upper side configuration yields a smooth and diffuse continuous water film, while the lower side configuration results in a partially thicker water film and incomplete water film coverage due to aggregation from uneven gravity distribution.

(a) (b)

(a) Upper side configuration (b) Lower side configuration

Fig. 14. The film formation of two configurations

Besides, the effect of heat and mass transfer on the water vapor content and channel temperature could also be easily analyzed. As shown in Fig. 15, the water vapor concentration in the secondary airflow in the wet channel of the upper side configuration is significantly higher than that in the lower side configuration. The mass transfer process between the water membrane and the airflow is smoother and faster, and the final water membrane transfers more mass to the airflow as a result. This is owing to the thinner and more uniform distribution of the water membrane covered on its plate surface.

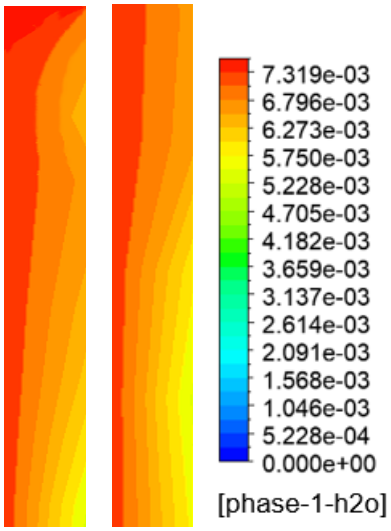

(a) Upper side configuration (b) Lower side configuration

Fig.15. The water vapor content distribution of two configurations

Correspondingly, Fig. 16 shows the temperature trends inside the wet channel for each of the two scenarios. It is clear that the temperature drop is stronger for the upper side configuration, reaching an average value of 25.5 ℃ at the outlet, while for another one it is 26.8 ℃. Such a result is based on the principle of IEC operation, where the evaporative heat absorption by the water film allows the secondary airflow to transfer heat to the water film thus achieving the desired temperature drop of the airflow. Corresponding to the upper analysis, the temperature drop is the same as the increasing trend of water vapor concentration. Furthermore, it is evident that the film temperature does not change due to the heat absorbed from the airflow.

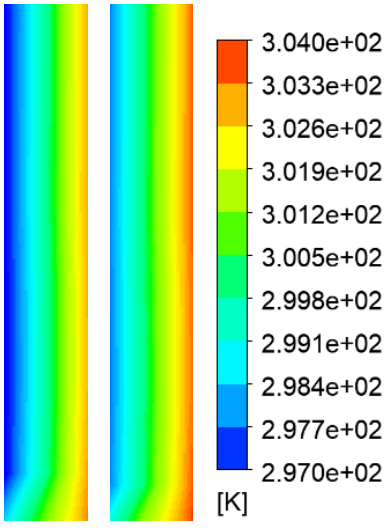

(a) Upper side configuration (b) Lower side configuration

Fig. 16. The temperature distribution of two configurations

4.2.5 Specific gaps in the four configurations

Moreover, Fig. 17 summarized the specific values of the water film coverage coefficient and the primary airflow temperature variation along the wet channel surface for the four cases. Obliviously, the temperature drop in the primary airflow typically follows the same trend as the water film coverage coefficient of the wet channel. The best results are achieved in the upper side configuration, while the water film coverage ratio and temperature drop are 0.76 and 24.1℃, respectively, with a 59.2% and 27.4% improvement compared to the worst configuration directly. In addition, a small expansion of the wetted area at such low wetting rates also leads to a relatively high temperature rise, while further optimization is no longer apparent when wetting is already more uniform and close to the maximum.

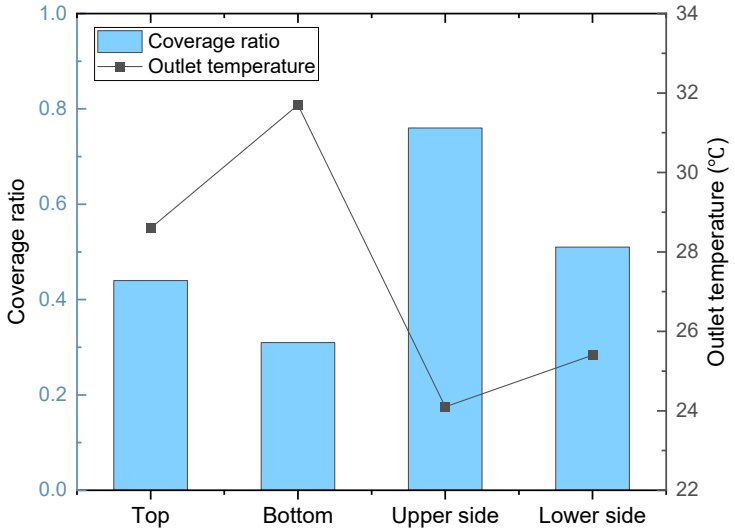

Fig. 17. The coverage ratio and outlet temperature of four configurations

5 Approaches for cooling performance enhancement

5.1 Performance enhancement by hydrophilic coating

The wettability of the plate surface inside IEC wet channel is determined by a combination of nozzle configurations and plate surface characteristics, while the contact angle is a crucial parameter for affecting the wetted area by water on a certain surface. In general, the three-phase equilibrium of the gas, liquid, as well as solid phases in the measuring environment determines the contact angle value. The interfacial tension of the water phase and the surface energy of the solid phase are what determine the contact angle, thus decreasing the interfacial tension of the liquid or rising the surface energy of the solid surface could enhance the wetting ratio of the descending film. Previous studies have shown that the addition of a new hydrophilic coating to the IEC wet channel surface can reduce the contact angle between the droplets and the heat exchanger plate surface, thus improving the uniformity of droplet distribution. Therefore, this section will further investigate and analyze the wet channel using standard epoxy resin coating and IEC with well-dispersed hydrophilic coating, respectively.

Firstly, the contact angles of the wet channel walls of IEC with conventional epoxy resin coating and new hydrophilic paint were determined to be 77.8° and 57.8°, respectively [56]. Then, the contact angle of the additional hydrophilic coating was applied as the initial setting parameter of the heat exchanger wet channel wall boundary by EWF setting in the simulation of the CFD model proposed in this study. Fig. 18 (a) demonstrates the water membrane distribution on the plate surface of the IEC wet channel with a coated counterflow arrangement. There is no doubt that the shrinkage of the descending membrane on the plate surface of the IEC wet channel is significantly reduced for a 20° reduction in contact angle, with a relative increase of 14.5% in water film coverage from 0.76 to 0.87. Correspondingly, the evaporative heat absorption phenomenon of the secondary airflow in the wet channel is also more adequate as exemplified in Fig. 18 (b). Consequently, the temperature drop response of the primary airflow is also greater, from 24.1℃ to 22.4℃, a relative increase of 7.4%. The improvement mechanism of the hydrophilic coated IEC is based on optimization for the contact state of water droplets and heat exchanger walls thus expanding the contact area and mass transfer area within the water film and the secondary airflow, the area of water in contact with the surface of the plate rises while the area available for evaporation of the water spray film is also enhanced. The end result is an increase in IEC wet-bulb efficiency and an overall increase in heat exchange capacity.

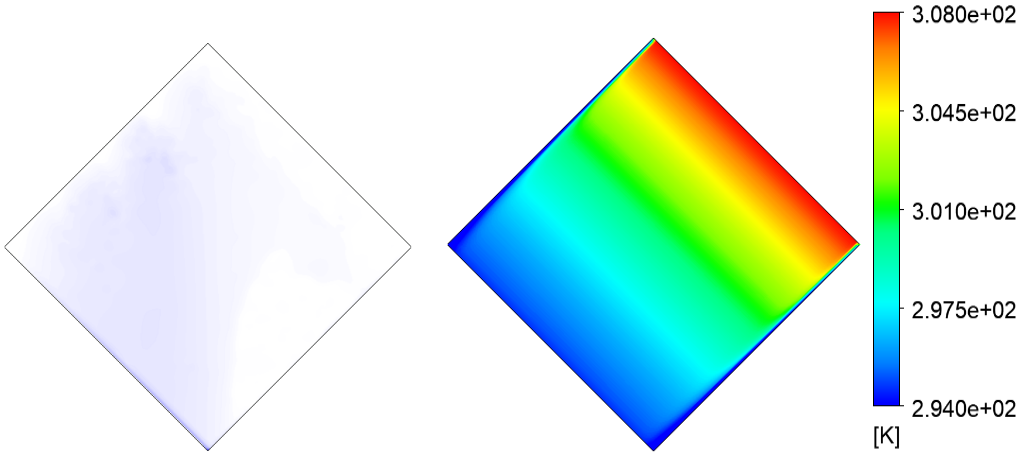

(a) Water film distribution (b) Temperature distribution of primary air

Fig. 18. The performance improved by hydrophilic coating

5.2 Performance enhancement by fiber coating

With the aim of improving the poor wetting of conventional aluminum and polymer IECs, another proven method is the proposal to attach a fiber coating to the walls of the IEC in order to enhance the wetting circumstances through its great water diffusion. The results showed that the fiber coating considerably improved the wetting conditions, with a contact angle of 0° between the spray droplets and the wall surface, and that the water film distribution as well as wetting rate on the surface of the plate were optimized [57]. The outlet air temperature of IEC can be left unaffected by the enhanced thermal resistance of the fiber covering when running in totally wet conditions. Maintaining the wet channel surface wetness is therefore a necessary condition for the use of fiber coatings. Additionally, to increasing surface wetness, the fiber coating has water conservation properties that make it possible to apply water spray for IEC intermittently.

Consequently, the ratio of water film coverage simulated in the IEC model based on the fiber coating can be considered as 1. Fig. 19 (a) elucidates the water membrane distribution in the diamond-shaped IEC wet channel with the additional fiber coating. Undoubtedly, with a contact angle of 0° and no water film shrinkage, the water film almost completely covers the heat exchanger wall from top to bottom, which is a 31.6% improvement compared to the original IEC with aluminum plate. In

addition, the temperature drops in the primary air indicated by Fig. 19 (b) is greater, from 24.1°C to 20.7°C, a relative increase of 16.4%. The improvement mechanism of the fiber-coated IEC is manifested in two ways: first, the distribution of the water film in the wet channel benefits from a more uniform distribution of the diffusion phenomenon of the fiber material than that of the hydrophilic coating; second, the water retention capacity of the fiber material ensures the possibility of indirect water injection, thus achieving lower power demand of pump and higher COP of IEC system.

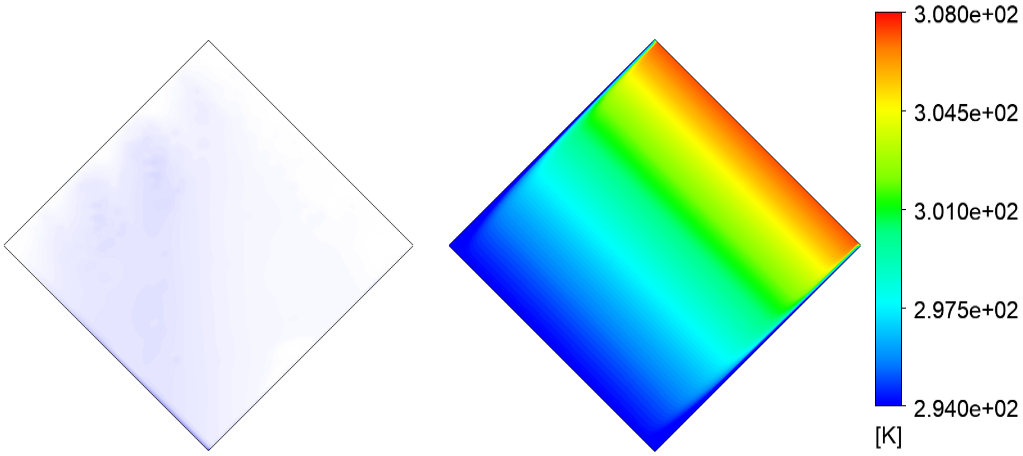

(a) Water film distribution (b) Temperature distribution of primary air

Fig. 19. The performance improved by fiber coating

5.3 Assessment of the degree of enhancement

Comparing the performance of the original solution with that of the two performance enhancement solutions, it is apparent that from the Fig. 20 (a) both the hydrophilic coating applied to the wet channel walls and the additional fiber coating increase the wetting ratio of the walls by decreasing the contact angle between the droplets and the wall surface. In addition, the fiber coating increases the diffusion rate of the water film compared to the hydrophilic one, thus achieving a wetting ratio close to 1, which is regarded as complete wetting. Accordingly, as shown in Fig. 20 (b), when the wetting rate is increased, the wetted surface of the wet channel has a larger contact area with the secondary air flow, the evaporation and heat absorption reaction is more intense and the temperature drop on the surface is more dramatic. As a consequence, the wet-bulb efficiency of the IEC was optimized for both the increased hydrophilic and fiber coating on the plate surface, by 5.7% and 14.5% respectively. Moreover, on account of the water conservation capacity of the fiber coating, which allows for indirect spraying, the energy requirement of the pump is reduced, resulting in a further increase in the COP value of 16.1%. Furthermore, due to the improved cooling capacity, the exergy efficiency of the diamond-shaped IEC with additional enhancement coating has been improved by 24.2% and 33.7% respectively without any other external energy consumption. Thus, the enhancement of the wetting ratio of the IEC wet channel by a functional coating, thus enhancing the evaporative heat absorption process, is always an effective way of heat transfer enhancement.

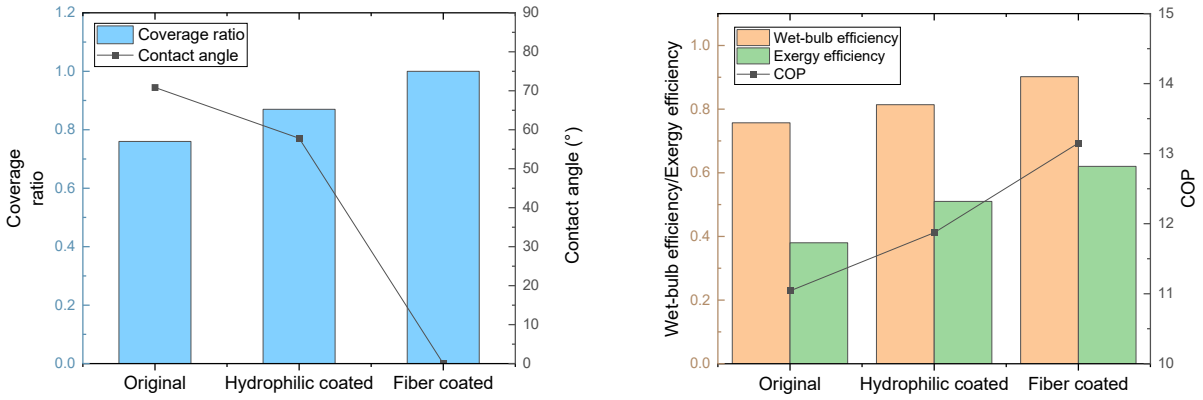

(a) Effect on coverage ratio and contact angle (b) Comparison of the three performance indexes

Fig. 20. The performance comparison among original, hydrophilic coating and fiber coating

6 Conclusions

The purpose of this research is to develop a CFD model to investigate the air-water flow, heat and mass transfer capabilities of a diamond-shaped IEC with the water spray system. By incorporating theoretical principles, computational domains, model verification and parameter analysis, the optimal nozzle configuration and performance were discovered. Several enhancement strategies, including hydrophilic coating and fiber coating, were also proposed. The enhancement of wet-bulb efficiency, exergy efficiency and COP value with characteristics as well as enhancement mechanisms were explained. The following is a summary and list of some concluding remarks:

1) With the IEC at a lower flow rate in the water supply system, the water film coverage reflects a more significant expand with the increase of the flow rate. However, when the water supply flow rate arrives 65 L/s, the water membrane coverage gradually stabilizes at the maximum value, and further increasing the flow rate does not benefit the wetting rate excepting increasing the power consumption of the pump.

2) Due to the nature of the IEC heat transfer mechanism, its performance is largely influenced by the surface wetting coefficient. For the diamond-shaped IEC, the nozzles are installed as upper side configuration when the water film distribution area in the wet channel is the largest and the temperature drop is the best, with 59.2% and 27.4% improvement over the worst case, respectively.

3) Benefit from the addition of hydrophilic coatings on the plate surface of wet channels, the contact angle between the water droplets and the plate surface is reduced, thus weakening the shrinkage effect of the water film, resulting in an increase in the water film coverage. Compared with the conventional aluminum plate IEC, the water film coverage and COP are increased by 14.5% and 7.4%, respectively.

4) Moreover, the diffusion-based properties of the fiber coating in addition to expanding the wetted area also make intermittent spraying of IEC possible, thus reducing the power consumption of the system. Compared to the initial solution, the water film coverage increased by 31.6% and the wet-bulb efficiency of IEC improved by 16.1%.

Declaration of Competing Interest

The authors declare that they have no known competing financial interests or personal relationships that could have appeared to influence the work reported in this paper.

CRediT authorship contribution statement

Xiaochen Ma: Conceptualization, Methodology, Experiment, Writing – original draft. **Wenchao Shi:** Validation, Resources, Formal analysis. **Hongxing Yang:** Conceptualization, Supervision, Funding acquisition, Writing – review & editing.

Acknowledgment

The authors wish to acknowledge the financial support provided by the two General Research Fund projects funded by the Hong Kong Research Grant Council (Ref. No.: 15213219 and 15200420).

References

[1] Liu X, Liu X, Jiang Y, Zhang T, Hao B. PEDF (photovoltaics, energy storage, directcurrent, flexibility), a power distributionsystemof buildings for grid decarbonization: definition,technology review, and application 2022. https://doi.org/10.17775/CSEEJPES.2022.04850.

[2] Wu T, Cao B, Zhu Y. A field study on thermal comfort and air-conditioning energy use in an office building in Guangzhou. Energy Build 2018;168:428–37. https://doi.org/10.1016/j.enbuild.2018.03.030.

[3] Min Y, Chen Y, Yang H, Guo C. Characteristics of primary air condensation in indirect evaporative cooler: Theoretical analysis and visualized validation. Build Environ 2020;174:106783. https://doi.org/10.1016/j.buildenv.2020.106783.

[4] Spandagos C, Ng TL. Equivalent full-load hours for assessing climate change impact on building cooling and heating energy consumption in large Asian cities. Appl Energy 2017;189:352–68. https://doi.org/10.1016/j.apenergy.2016.12.039.

[5] Ebrahimi K, Jones GF, Fleischer AS. A review of data center cooling technology, operating conditions and the corresponding low-grade waste heat recovery opportunities. Renew Sustain Energy Rev 2014;31:622–38. https://doi.org/10.1016/j.rser.2013.12.007.

[6] Chua KJ, Chou SK, Yang WM, Yan J. Achieving better energy-efficient air conditioning - A review of technologies and strategies. Appl Energy 2013;104:87–104. https://doi.org/10.1016/j.apenergy.2012.10.037.

[7] Shi W, Yang H, Ma X, Liu X. Techno-economic evaluation and environmental benefit of hybrid evaporative cooling system in hot-humid regions. Sustain Cities Soc 2023:104735. https://doi.org/10.1016/j.scs.2023.104735.

[8] Yang H, Shi W, Chen Y, Min Y. Research development of indirect evaporative cooling technology: An updated review. Renew Sustain Energy Rev 2021;145:111082. https://doi.org/10.1016/j.rser.2021.111082.

[9] Moshari S, Heidarinejad G, Fathipour A. Numerical investigation of wet-bulb effectiveness and water consumption in one-and two-stage indirect evaporative coolers. Energy Convers Manag 2016;108:309–21. https://doi.org/10.1016/j.enconman.2015.11.022.

[10] AS D. Future ready modular data centre solutions for DigiPlex 2020:1–2.

[11] Will your IT withstand a sustainability review ? n.d.

[12] Zhichao G, Xiang H, Jianli S, Junjie C. Indirect evaporative cooling air conditioning systems in domestic and international data centres 2017:1–6.

[13] Chenyu J, Xiang H, Zhenwu T, Zhenyu L YJ. Study on the application of indirect evaporative cooling technology in domestic and international data centres. Refrig Air-Conditioning 2020;1:61–7.

[14] Chu J, Huang X. Research status and development trends of evaporative cooling air-conditioning technology in data centers. Energy Built Environ 2023;4:86–110. https://doi.org/10.1016/j.enbenv.2021.08.004.

[15] Cui X, Mohan B, Islam MR, Chua KJ. Investigating the energy performance of an air treatment incorporated cooling system for hot and humid climate. Energy Build 2017;151:217–27. https://doi.org/10.1016/j.enbuild.2017.06.059.

[16] Min Y, Chen Y, Yang H. Numerical study on indirect evaporative coolers considering condensation: A thorough comparison between cross flow and counter flow. Int J Heat Mass Transf 2019;131:472–86. https://doi.org/10.1016/j.ijheatmasstransfer.2018.11.082.

[17] Chen Y, Yang H, Luo Y. Indirect evaporative cooler considering condensation from primary air: Model development and parameter analysis. Build Environ 2016;95:330–45. https://doi.org/10.1016/j.buildenv.2015.09.030.

[18] Chen Y, Yang H, Luo Y. Parameter sensitivity analysis and configuration optimization of indirect evaporative cooler (IEC) considering condensation. Appl Energy 2017;194:440–53. https://doi.org/10.1016/j.apenergy.2016.06.121.

[19] Boukhanouf R, Amer O, Ibrahim H, Calautit J. Design and performance analysis of a regenerative evaporative cooler for cooling of buildings in arid climates. Build Environ 2018;142:1–10. https://doi.org/10.1016/j.buildenv.2018.06.004.

[20] Al-Zubaydi AYT, Hong G. Experimental study of a novel water-spraying configuration in indirect evaporative cooling. Appl Therm Eng 2019;151:283–93. https://doi.org/10.1016/j.applthermaleng.2019.02.019.

[21] Ma X, Shi W, Yang H. Study on water spraying distribution to improve the energy recovery performance of indirect evaporative coolers with nozzle arrangement optimization. Appl Energy 2022;318:1–6. https://doi.org/10.1016/j.apenergy.2022.119212.

[22] Nie J, Yuan S, Fang L, Zhang Q, Li D. Experimental study on an innovative enthalpy recovery technology based on indirect flash evaporative cooling. Appl Therm Eng 2018;129:22–30. https://doi.org/10.1016/j.applthermaleng.2017.09.139.

[23] Adam A, Han D, He W, Amidpour M. Analysis of indirect evaporative cooler performance under various heat and mass exchanger dimensions and flow parameters. Int J Heat Mass Transf 2021;176:121299. https://doi.org/10.1016/j.ijheatmasstransfer.2021.121299.

[24] Heidarinejad, G., & Moshari, S. (2015). Novel modeling of an indirect evaporative cooling system with cross-flow configuration. Energy and Buildings, 92, 351-362.

[25] Anisimov, S., & Pandelidis, D. (2015). Theoretical study of the basic cycles for indirect evaporative air cooling. International Journal of Heat and Mass Transfer, 84, 974-989.

[26] Anisimov, S., Pandelidis, D., & Danielewicz, J. (2015). Numerical study and optimization of the combined indirect evaporative air cooler for air-conditioning systems. Energy, 80, 452-

464.

[27] Anisimov, S., Pandelidis, D., Jedlikowski, A., & Polushkin, V. (2014). Performance investigation of a M (Maisotsenko)-cycle cross-flow heat exchanger used for indirect evaporative cooling. Energy, 76, 593-606.

[28] Ren. C, Zhang. L. (2005). Three-dimensional Numerical Simulation indirect evaporative cooler by CFD. Energy Conservation. (6), 14-17. (In Chinese).

[29] Ding. J, Ren. C. (2006). Study on the Laminar Properties of Indirect Evaporative Cooling in Plate Heat Exchanger. Industrial heating, 35(2), 24-28. (in Chinese).

[30] Ding. J, Ren. C. (2007). Study on heat and mass transfer coefficient of indirect evaporative cooling in plate heat exchanger. Building Energy & Environment, 26(5), 1-6. (in Chinese).

[31] Cui X, Chua KJ, Yang WM, Ng KC, Thu K, Nguyen VT. Studying the performance of an improved dew-point evaporative design for cooling application. Appl Therm Eng 2014;63:624–33. https://doi.org/10.1016/j.applthermaleng.2013.11.070.

[32] Xu P, Ma X, Diallo TMO, Zhao X, Fancey K, Li D, et al. Numerical investigation of the energy performance of a guideless irregular heat and mass exchanger with corrugated heat transfer surface for dew point cooling. Energy 2016;109:803–17. https://doi.org/10.1016/j.energy.2016.05.062.

[33] You Y, Jiang H, Lv J. Analysis of influence of IEC heat exchanger based on CFD method. Energy Procedia 2019;158:5759–64. https://doi.org/10.1016/j.egypro.2019.01.555.

[34] Wan Y, Ren C, Xing L. An approach to the analysis of heat and mass transfer characteristics in indirect evaporative cooling with counter flow configurations. Int J Heat Mass Transf 2017;108:1750–63. https://doi.org/10.1016/j.ijheatmasstransfer.2017.01.019.

[35] Shi W, Min Y, Chen Y, Yang H. Development of a three-dimensional numerical model of indirect evaporative cooler incorporating with air dehumidification. Int J Heat Mass Transf 2022;185:122316. https://doi.org/10.1016/j.ijheatmasstransfer.2021.122316.

[36] Moshari S, Heidarinejad G. Analytical estimation of pressure drop in indirect evaporative coolers for power reduction. Energy Build 2017;150:149–62. https://doi.org/10.1016/j.enbuild.2017.05.080.

[37] Farmahini-farahani M, Pasdarshahri H. Exergy Analysis of Evaporative Cooling for Optimum Energy Consumption in Diverse Climate Conditions 2011;3:9–20.

[38] Berning T, Sørensen H, Nielsen MP. A COMPUTATIONAL FLUID DYNAMICS ANALYSIS OF AN INDIRECT EVAPORATIVE COOLER EMPLOYING THE PARTICLE TRANSPORT METHOD 2019:2–6.

[39] Haghshenas Fard M, Zivdar M, Rahimi R, Esfahany MN, Afacan A, Nandakumar K, et al. CFD simulation of mass transfer efficiency and pressure drop in a structured packed distillation column. Chem Eng Technol 2007;30:854–61. https://doi.org/10.1002/ceat.200700011.

[40] Tao W, Yimo L, Lin L. A novel 3D simulation model for investigating liquid desiccant dehumidification performance based on CFD technology. Appl Energy 2019;240:486–98. https://doi.org/10.1016/j.apenergy.2019.02.068.

[41] Gu F, Liu CJ, Yuan XG, Yu GC. CFD simulation of liquid film flow on inclined plates. Chem Eng Technol 2004;27:1099–104. https://doi.org/10.1002/ceat.200402018.

[42] Adam A, Han D, He W, Shi Q, Chen J, Zhong H. The influences of the plate shape on the

performance of the indirect evaporative cooler based on the CFD approach. J Brazilian Soc Mech Sci Eng 2023;45:1–14. https://doi.org/10.1007/s40430-023-04044-w.

[43] Sadighi Dizaji H, Hu EJ, Chen L, Pourhedayat S. Analytical/experimental sensitivity study of key design and operational parameters of perforated Maisotsenko cooler based on novel wet-surface theory. Appl Energy 2020;262:114557. https://doi.org/10.1016/j.apenergy.2020.114557.

[44] Shi W, Min Y, Ma X, Chen Y, Yang H. Dynamic performance evaluation of porous indirect evaporative cooling system with intermittent spraying strategies. Appl Energy 2022;311:118598. https://doi.org/10.1016/j.apenergy.2022.118598.

[45] Shi W, Ma X, Gu Y, Min Y, Yang H. Indirect evaporative cooling maps of China: Optimal and quick performance identification based on a data-driven model. Energy Convers Manag 2022;268. https://doi.org/10.1016/j.enconman.2022.116047.

[46] Kong XQ, Wang RZ, Huang XH. Energy efficiency and economic feasibility of CCHP driven by stirling engine. Energy Convers Manag 2004;45:1433–42. https://doi.org/10.1016/j.enconman.2003.09.009.

[47] Wang L, Zhan C, Zhang J, Zhao X. The energy and exergy analysis on the performance of counter-flow heat and mass exchanger for M-Cycle indirect evaporative cooling. Therm Sci 2019;23:613–23. https://doi.org/10.2298/TSCI171221153W.

[48] Yang Y, Ren C, Yang C, Tu M, Luo B, Fu J. Energy and exergy performance comparison of conventional, dew point and new external-cooling indirect evaporative coolers. Energy Convers Manag 2021;230:113824. https://doi.org/10.1016/j.enconman.2021.113824.

[49] Shi W, Yang H, Ma X, Liu X,. A novel indirect evaporative cooler with porous media under dual spraying modes: A comparative analysis from energy, exergy, and environmental perspectives. Journal of Building Engineering 2023. 106874. https://doi.org/10.1016/j.jobe.2023.106874.

[50] De Antonellis S, Joppolo CM, Liberati P. Performance measurement of a cross-flow indirect evaporative cooler: Effect of water nozzles and airflows arrangement. Energy Build 2019;184:114–21. https://doi.org/10.1016/j.enbuild.2018.11.049.

[51] Stoitchkov NJ, Dimitrov GI. Effectiveness of crossflow plate heat exchanger for indirect evaporative cooling: Efficacité des échangeurs thermiques à plaques, à courants croises pour refroidissement indirect évaporatif. Int J Refrig 1998;21:463–71.

[52] Dong C, Qi R, Zhang L, Lu L. Performance enhancement of solar-assisted liquid desiccant dehumidifiers using super-hydrophilic surface. Energy Build 2019;199:461–71. https://doi.org/10.1016/j.enbuild.2019.07.027.

[53] Dong C, Lu L, Wang X. Experimental investigation on non-boiling heat transfer of two-component air-oil and air-water slug flow in horizontal pipes. Int J Multiph Flow 2019;119:28–41. https://doi.org/10.1016/j.ijmultiphaseflow.2019.07.004.

[54] Jain M, John B, Iyer KN, Prabhu S V. Characterization of the full cone pressure swirl spray nozzles for the nuclear reactor containment spray system. Nucl Eng Des 2014;273:131–42. https://doi.org/10.1016/j.nucengdes.2014.02.025.

[55] Jain M, John B, Iyer KN, Prabhu S V. Characterization of the full cone pressure swirl spray nozzles for the nuclear reactor containment spray system. Nucl Eng Des 2014;273:131–42. https://doi.org/10.1016/j.nucengdes.2014.02.025.

[56] Guilizzoni M, Milani S, Liberati P, De Antonellis S. Effect of plates coating on performance

of an indirect evaporative cooling system. Int J Refrig 2019;104:367–75. https://doi.org/10.1016/j.ijrefrig.2019.05.029.

[57] Chen Y, Yan H, Min Y. Visualized study of wetting enhancement and thermal performance of fiber-coated indirect evaporative cooler. Appl Therm Eng 2023;221:119904. https://doi.org/10.1016/j.applthermaleng.2022.119904.